

Generative diffusion learning for parametric partial differential equations

Ting Wang^{1,3}, Petr Plecháč², and Jaroslav Knap³

¹Booz Allen Hamilton Inc.
wang_ting@bah.com

²Department of Mathematical Sciences, University of Delaware
plechac@udel.edu

³Physical Modeling and Simulation Branch, DEVCOM Army Research Laboratory
jaroslav.knap.civ@army.mil

Abstract

We develop a class of data-driven generative models that approximate the solution operator for parameter-dependent partial differential equations (PDE). We propose a novel probabilistic formulation of the operator learning problem based on recently developed generative denoising diffusion probabilistic models (DDPM) in order to learn the input-to-output mapping between problem parameters and solutions of the PDE. To achieve this goal we modify DDPM to supervised learning in which the solution operator for the PDE is represented by a class of conditional distributions. The probabilistic formulation combined with DDPM allows for an automatic quantification of confidence intervals for the learned solutions. Furthermore, the framework is directly applicable for learning from a noisy data set. We compare computational performance of the developed method with the Fourier Network Operators (FNO). Our results show that our method achieves comparable accuracy and recovers the noise magnitude when applied to data sets with outputs corrupted by additive noise.

1 Introduction

In many scientific and engineering applications, it is essential to handle computational models involving random input parameters. Often this task is computationally challenging as it relies on repeated solves of the underlying mathematical model for distinct values of input parameters. It is therefore crucial to develop fast and reliable methods that solve the problems for a range of input parameters.

Operator learning problem. In the context of parameter dependent partial differential equations (PDEs) the reliance of a solution on input parameters can be conveniently captured by the the following abstract PDE

$$\mathcal{F}(u(x); a(x)) = 0, \quad \text{in } D \subset \mathbb{R}^d, \quad (1)$$

defined by the mapping $\mathcal{F} : \mathcal{U} \times \mathcal{A} \rightarrow \mathbb{R}$. Here \mathcal{A} and \mathcal{U} are suitable spaces of functions over the domain D for which the problem is well-posed. The input a takes values in the input function space \mathcal{A} and u is the corresponding solution taking values in the output function space \mathcal{U} . A typical example where the proposed approach will be applied is the case when a is a random field distributed according to a probability measure μ . We give specific examples of PDEs later when discussing various benchmarks. For now we tacitly assume that the choice of \mathcal{F} , \mathcal{A} , \mathcal{U} , and \mathcal{V} defines a well-posed problem. In other words, we assume that there exists a unique solution operator, or equivalently

input-to-output mapping $\mathcal{S} : \mathcal{A} \rightarrow \mathcal{U}$ such that $u = \mathcal{S}(a)$ is uniquely defined and stable in the respective topology of the space \mathcal{A} and \mathcal{U} . The overarching goal of the operator learning problem is to find an operator $\mathcal{S}_\theta : \mathcal{A} \rightarrow \mathcal{U}$, parameterized by the parameters θ , and approximating \mathcal{S} in a certain sense. Once \mathcal{S}_θ is learned, solutions to (1) can be readily evaluated for a range of inputs thus avoiding repeated solves of the equation for different a .

We emphasize that the function spaces \mathcal{A} and \mathcal{U} are infinite dimensional by definition. However, in the numerical context we only have access to the pair of fields (a, u) in some finite dimensional approximation spaces \mathcal{A}_M and \mathcal{U}_M . For example, on a discretization of the domain D with an M^d points grid, i.e., $D_M \subset D$. With a slight abuse the notation, in the remainder of the article we denote $a = a|_{D_M} \in \mathcal{A}_M = \mathbb{R}^{M^d \times d_a}$ and $u = u|_{D_M} \in \mathcal{U}_M = \mathbb{R}^{M^d \times d_u}$. For the ease of presentation, we assume that the function spaces \mathcal{A} and \mathcal{U} are real-valued and hence $d_a = d_u = 1$.

Operator learning methods. Modern machine learning techniques provide a promising tool for tackling the operator learning problem. Current neural network based operator learning methods can be classified into two categories: purely data driven and physics informed. The data-driven approach assumes the access to a data set of input-output pairs $\mathcal{D} = \{(a^{(n)}, u^{(n)})\}_{n=1}^N$ and aims to learn the parametric approximation \mathcal{S}_θ , such that the empirical data loss function

$$\mathcal{L}_{\text{DD}}(\theta) = \frac{1}{N} \sum_{n=1}^N \|u^{(n)} - \mathcal{S}_\theta(a^{(n)})\|^2 \quad (2)$$

is minimized over the space of parameters θ . Recently, various deep learning architectures have been designed in order to solve (2) efficiently. The state-of-the-art methods, e.g., the fully convolution network [33], PCA network [2, 7], multi-wavelet method [6], turbulent flow net [27], deep operator net (ONet) [16, 17], and the Fourier neural operator (FNO) [12, 13, 14], etc., all fall into this category. Among them, ONet approximates the solution operator based on the universal approximation theorem of operators [3] and FNO parameterizes the integral kernel directly in Fourier space [11]. Both methods have received tremendous attention thanks to their mesh independent feature. Other than the above mentioned deep learning based methods, we also refer the reader to a recent work on a kernel-based framework for operator learning [1]. Although the data-driven approach shows promising performance in solving many challenging parametric PDE problems, it still faces the main limitation of being data-intensive.

In comparison, the physics-informed approach relies on the direct knowledge of the underlying PDE in order to learn \mathcal{S}_θ and utilizes the physics-informed empirical loss in the minimal residual form

$$\mathcal{L}_{\text{PI}}(\theta) = \frac{1}{N} \sum_{n=1}^N \|\mathcal{F}(\mathcal{S}_\theta(a^{(n)}); a^{(n)})\|^2. \quad (3)$$

Since the above loss only involves the input a and not the solution (output) u , the physics-informed approach, in principle, does not require the knowledge of the data set \mathcal{D} and hence has the key advantage of being “data-free” by design [15, 18, 29, 31, 34]. Nevertheless, the optimization of a physics-informed loss remains challenging and consequently limits its applicability to relatively simple problems [26, 28, 30]. We emphasize that all the methods mentioned above learn an operator \mathcal{S}_θ that is inherently deterministic since it maps a given input realization a to a unique output realization $u = \mathcal{S}_\theta(a)$.

Denosing diffusion probabilistic model. Recently, DDPM has outperformed traditional deep generative models in image synthesis thanks to its ability to generate high quality samples from complex and high dimensional distributions [5, 8, 22, 24]. Inspired by sampling technique from non-equilibrium thermodynamics, DDPM utilizes the time reversal property of a class of parameterized Markov chains in order to learn a sequence of latent distributions that eventually converge to the data distribution [25]. Once properly trained, the model sequentially transforms a given Gaussian noise into a sample from the data distribution.

Contributions of our work. Based on DDPM, we introduce a probabilistic method, termed as the *probabilistic diffusion neural operator* (PDNO), for solving the operator learning problem.

- To achieve this, we propose a probabilistic formulation of the operator learning problem by reformulating it as a conditional distribution learning problem, i.e., given an input a , we learn a generative model for the conditional distribution $u|a$.
- The proposed formulation allows a natural application of DDPM as the underlying sampler for $u|a$. To the best of our knowledge, this is the first work employing DDPM for the operator learning problem.
- Since our method maximizes the evidence likelihood and it learns a class of distributions $u|a$, it is directly applicable to a noisy data set where the output $u|a$ is beyond a Dirac distribution (i.e., when u is noise free). Moreover, the learned standard deviation (std) of $u|a$ provides an informative quantification of the uncertainty and hence the predictive quality of the learned model.
- In comparison with FNO or ONet, our method requires fewer regularity assumptions in addition to DDPM being well-known for its flexibility as a generative model when learning complex distributions. Hence, we anticipate the method being capable of learning highly non-smooth solutions (see the advection PDE example in Section 4).

The main goal of this work is to explore what possibilities DDPM can offer in computational science. Our numerical experiments in Section 4 suggest that PDNO can be a promising complement to the data-driven approach for operator learning. Despite the advantages summarized above, the current method does suffer certain limitations compared to state-of-the-art methods such as FNO and ONet. We discuss these limitations in detail in the conclusion section.

2 The probabilistic formulation

The starting point of our method for solving the operator learning problem is to view each output u for a given input a as a conditional random variable. Such a viewpoint naturally leads to the probabilistic formulation: to learn a probabilistic conditional model $q_\theta(u|a)$ by maximizing the joint data likelihood $q_\theta(\mathcal{D})$. Since the input distribution of $a \sim \mu$ is known, this is equivalent to maximizing the following conditional likelihood

$$\prod_{n=1}^N q_\theta(u^{(n)}|a^{(n)}) \propto q_\theta(\mathcal{D}) = \prod_{n=1}^N q_\theta(u^{(n)}|a^{(n)})p(a^{(n)}). \quad (4)$$

Although for a given input a the corresponding output u , as a solution to the PDE (1), is deterministic, there is no loss of generality in modeling it as random since $u|a$ can be viewed as a Dirac measure $\delta_u(\cdot|a)$ concentrated at the solution u if no noise is added to u . Indeed, solving a deterministic problem from a stochastic perspective is common in machine learning, e.g., Gaussian process regression uses a Gaussian random field to describe a distribution over functions [32].

The advantage of the probabilistic approach for operator learning is two-fold: (i) *Flexibility*: the probabilistic model $q_\theta(u|a)$ is more flexible than deterministic models since it does not depend on the specific choice of the cost functional \mathcal{L} . For instance, we can assume that the prediction $\mathcal{S}_\theta(a)$ and the observation u differ by a Gaussian noise ϵ , i.e., $u = \mathcal{S}_\theta(a) + \epsilon$ with $\epsilon \sim \mathcal{N}(0, \sigma_n^2 \mathbf{I})$. Note that when the noise magnitude σ_n is known, maximizing the likelihood (4) leads to (2) with \mathcal{L} being the L_2 -loss. In this work, we do not assume any distribution for the conditional $q_\theta(u|a)$ but rather learn it completely from the data in a generative manner. (ii) *Uncertainty evaluation*: in practice the data can contain noise due to numerical/measurement errors and similarly the trained model can demonstrate uncertainty due to over-fitting or under-fitting. Aside from the prediction of the output, we are often interested in the quality of the prediction as well. The probabilistic model $q_\theta(\cdot|a)$ allows for quantifying uncertainty of the learned model arising from data sets corrupted by noise.

Since our probabilistic framework constructs the conditional distribution $q_\theta(u|a)$, it is directly applicable to the noisy data setting as well and hence we consider two types of data sets in this work: **1) Noise-free data**: for each input a , there is a unique output u in the noise-free data set \mathcal{D} such that the pair (a, u) solves (1). Therefore, our probabilistic model $q_\theta(u|a)$ learns a class of Dirac distributions $\delta_u(\cdot|a)$; **2) Gaussian noise data**: we assume a noisy data set \mathcal{D}_η obtained from corrupting the output u by an additive Gaussian noise $\eta \sim \mathcal{N}(0, \Sigma(a))$, i.e., $u_\eta = u + \eta$. In this case, the data set may contain repeated realizations of a whose corresponding outputs u_η are different due to the noise. Therefore, our probabilistic model $q_\theta(u|a)$ learns a Gaussian distribution $\mathcal{N}(u; m(a), \Sigma(a))$. Note that we do not assume the covariance $\Sigma(a)$ is known and hence the maximum likelihood estimation (4) is not equivalent to minimizing the L_2 -loss (2).

3 Conditional DDPM for operator learning

The specific model that we apply in learning the distribution $q_\theta(u|a)$ is the DDPM, which fits naturally as a sampler with the proposed probabilistic framework. We first briefly review the basic framework for the unconditional DDPM and then generalize it to the conditional setting.

3.1 Denoising diffusion probabilistic model

Given a set of unlabeled observations of u , a DDPM learns a sampler of the underlying distribution $p(u)$ by constructing a time reversible Markov chain. Specifically, DDPM views the observation u as an initial state u_0 of a Markov chain defined by the forward transition probability

$$p(u_t|u_{t-1}) = \mathcal{N}(u_t; \sqrt{1 - \beta_t}u_{t-1}, \beta_t \mathbf{I}), \quad t = 1, \dots, T \quad (5)$$

where β_t is the variance schedule such that the final state u_T is approximately standard normal for T sufficiently large. The joint distribution of the Markov chain (conditioned on u_0) is hence given by

$$p(u_{1:T}|u_0) = \prod_{t=1}^T p(u_t|u_{t-1}). \quad (6)$$

The process $u_{1:T}$ can be considered as a procedure of gradually adding noise to u_0 until it becomes a Gaussian noise u_T . Conversely, we can start from a normal distribution $q_\theta(u_T)$ and gradually denoise it to obtain the desired distribution $q_\theta(u_0) \approx p(u_0)$. This is accomplished by defining the reverse transition probability

$$q_\theta(u_{t-1}|u_t) = \mathcal{N}(u_{t-1}; m_\theta(t, u_t), \Sigma_\theta(t, u_t)), \quad t = T, \dots, 1, \quad (7)$$

where $m_\theta(t, u_t)$ and $\Sigma_\theta(t, u_t)$ are the mean and the covariance of the distribution, respectively. The joint distribution of the reverse Markov chain is hence given by

$$q_\theta(u_{0:T}) = q_\theta(u_T) \prod_{t=1}^T q_\theta(u_{t-1}|u_t). \quad (8)$$

The DDPM parameterizes m_θ and Σ_θ using neural networks in order to maximize the log-likelihood $\log q_\theta(u_0)$. Due to the intractability of the likelihood, the training is performed by maximizing the usual variational lower bound (VLB)

$$-\log q_\theta(u_0) \leq -\text{VLB}(\theta) \triangleq \mathbb{E}_{p(u_{0:T})} \left[\log \frac{p(u_{1:T}|u_0)}{q_\theta(u_{0:T})} \right].$$

Once we learn the reversed model q_θ , we can sample from $q_\theta(u_0) \approx p(u_0)$ by running the reverse time Markov chain from time T to 0.

3.2 Conditional DDPM

Recall that we are given a data set of input-output pairs \mathcal{D} and we aim at learning the conditional distribution $q_\theta(u|a)$. To adapt the DDPM to supervised learning, we let the initial state u_0 depend on the input a and define the conditional forward transition distribution

$$p(u_t|u_{t-1}, a) = \mathcal{N}(u_t; \sqrt{1 - \beta_t}u_{t-1}, \beta_t \mathbf{I}), \quad t = 1, \dots, T. \quad (9)$$

Note that the above conditional transition distribution remains the same as the unconditional one (5). However, the input a does affect the parameterization of the conditional reverse transition distribution

$$q_\theta(u_{t-1}|u_t, a) = \mathcal{N}(u_{t-1}; m_\theta(t, u_t, a), \Sigma_\theta(t, u_t, a)), \quad (10)$$

where $m_\theta(t, u_t, a)$ and $\Sigma_\theta(t, u_t, a)$ are the mean and the covariance whose parameterization will be worked in next section. This can be seen from the Bayes' formula that the true conditional reverse transition distribution

$$p(u_{t-1}|u_t, a) = \frac{p(u_t|u_{t-1}, a)p(u_{t-1}|a)}{p(u_t|a)}$$

depends on a as both $p(u_{t-1}|a)$ and $p(u_t|a)$ depend on a . Similar to the unconditional DDPM, we perform the training by maximizing the VLB of the conditional log likelihood

$$-\log q_\theta(u_0|a) \leq -\text{VLB}(\theta; a) \triangleq \mathbb{E}_{p(u_{0:T}|a)} \left[\log \frac{p(u_{1:T}|u_0)}{q_\theta(u_{0:T}|a)} \right].$$

To derive a computable form of the VLB, we mimic the unconditional PPDM and write

$$-\text{VLB} = L_T + \sum_{t=2}^T L_{t-1} + L_0, \quad (11)$$

where

$$\begin{aligned} L_0(\theta; a) &= \mathbb{E}_{p(u_1|a)} [-\log q_\theta(u_0|u_1, a)] \\ L_{t-1}(\theta; a) &= \mathbb{E}_{p(u_t, u_0|a)} [\text{KL}(p(u_{t-1}|u_t, u_0) || q_\theta(u_{t-1}|u_t, a))], \quad t = 2, \dots, T \\ L_T(\theta; a) &= \mathbb{E}_{p(u_0|a)} [\text{KL}(p(u_T|u_0) || q_\theta(u_T))]. \end{aligned}$$

For completeness, we show the derivation of (11) in Appendix B.1. Since $q_\theta(u_T)$ is assumed to be a standard Gaussian, L_T is independent of the parameter θ .

3.3 Parameterization for the reverse process

In order to minimize L_{t-1} for $t = 2, \dots, T$, we first apply Bayes' formula and the reparameterization trick to obtain

$$p(u_{t-1}|u_t, u_0) = \mathcal{N}(u_{t-1}; m(t, u_t, u_0), \Sigma(t, u_t, u_0)), \quad (12)$$

with

$$m(t, u_t, u_0) = \frac{1}{\sqrt{\alpha_t}} \left(u_t - \frac{1 - \alpha_t}{\sqrt{1 - \alpha_t}} \epsilon_t \right), \quad \Sigma(t, u_t, u_0) = \frac{1 - \bar{\alpha}_{t-1}}{1 - \bar{\alpha}_t} \beta_t \mathbf{I},$$

where $\bar{\alpha}_t = \prod_{n=1}^t \alpha_n$ with $\alpha_t = 1 - \beta_t$ and ϵ_t is a standard Gaussian (see Appendix B.2 for derivation). Note that the covariance $\Sigma(t, u_t, u_0)$ only depends on the time t but not the state u_t and u_0 . Next, we parameterize $q_\theta(u_{t-1}|u_t, a)$ so that it is of the same form as $p(u_{t-1}|u_t, u_0)$. Following the unconditional DDPM, we choose the following parametric form

$$q_\theta(u_{t-1}|u_t, a) = \mathcal{N}(u_{t-1}; m_\theta(t, u_t, a), \Sigma_\theta(t, u_t, a)) \quad (13)$$

with

$$m_\theta(t, u_t, a) = \frac{1}{\sqrt{\alpha_t}} \left(u_t - \frac{1 - \alpha_t}{\sqrt{1 - \bar{\alpha}_t}} \epsilon_\theta(t, u_t, a) \right),$$

where $\epsilon_\theta(t, u_t, a)$ is a neural network function that approximates the standard Gaussian ϵ_t . The choice of the covariance depends on the data distribution as follows

$$\Sigma_\theta(t, u_t, a) = \begin{cases} \frac{1 - \bar{\alpha}_{t-1}}{1 - \bar{\alpha}_t} \beta_t \mathbf{I} & \text{Noise free observation,} \\ \beta_t \mathbf{I} & \text{Observations with additive Gaussian noise.} \end{cases} \quad (14)$$

In the case of data set with non-Gaussian noise, a linear combination of the above two covariances can be used for introducing an additional hyper-parameter λ . Note that $\Sigma_\theta(t, u_t, a)$ in (14) is indeed not parameterized by θ and is independent of u_t and a . Comparing the two distributions (12) and (13) in KL divergence and empirically ignoring the pre-factor lead to

$$L_{t-1}(\theta) = \mathbb{E}_{p(\epsilon_t)p(u_0|a)} [\|\epsilon_t - \epsilon_\theta(t, \sqrt{\alpha_t}u_0 + \sqrt{1 - \bar{\alpha}_t}\epsilon_t, a)\|^2], \quad t = 2, \dots, T, \quad (15)$$

where we have replaced u_t by (B.1) using the reparameterization trick. Similarly, we can calculate L_0 and ignore the pre-factor which gives

$$L_0(\theta) = \mathbb{E}_{p(\epsilon_1)p(u_0|a)} [\|\epsilon_1 - \epsilon_\theta(1, \sqrt{\bar{\alpha}_1}u_0 + \sqrt{1 - \bar{\alpha}_1}\epsilon_1, a)\|^2]. \quad (16)$$

Unifying (15) and (16) and averaging over the input a leads to the final loss function to be optimized:

$$L(\theta) = \mathbb{E}_{t \sim \text{Unif}(1, \dots, T)} \mathbb{E}_{p(a, u_0)} \mathbb{E}_{p(\epsilon_t)} [\|\epsilon_t - \epsilon_\theta(t, \sqrt{\alpha_t}u_0 + \sqrt{1 - \bar{\alpha}_t}\epsilon_t, a)\|^2], \quad (17)$$

where ϵ_t are i. i. d. standard Gaussians.

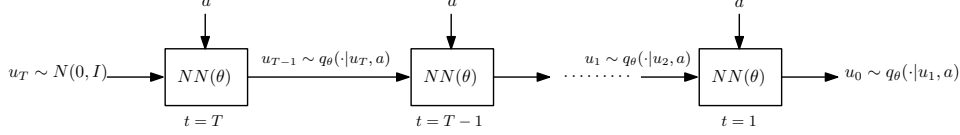


Figure 1: A schematic diagram of the inference stage of PDNO

3.4 Probabilistic diffusion neural operator

The resulting PDNO algorithm consists of two stages: the training stage that minimizes $L(\theta)$ in order to learn the reversed conditional Markov model $q_\theta(u_{t-1}|u_t, a)$ and the inference stage that samples sequentially from $q_\theta(u_{t-1}|u_t, a)$, as depicted in the schematic diagram 1. Algorithm 1 summarizes the procedure for training and sampling of PDNO. As indicated in (13), we parameterize the noise predictor ϵ_θ for $q_\theta(u_{t-1}|u_t, a)$, which has been empirically observed to produce higher accuracy than parameterizing the mean m_θ directly. For implementation, we follow the architecture presented in [8] to use a UNet backbone to represent the noise predictor $\epsilon_\theta(t, u_t, a)$ with the sinusoidal position embedding for t [21]. In comparison with the unconditional DDPM, the conditional DDPM utilized by PDNO takes an additional argument a as the input to the UNet. In our implementation, a and u_t are channel-wise concatenated before being fed into the UNet.

Algorithm 1 PDNO

Training Stage:

- 1: **repeat**
- 2: $(a, u) \sim p(a, u)$
- 3: $t \sim \text{Unif}(1, \dots, T)$
- 4: $\epsilon \sim \mathcal{N}(0, I)$
- 5: stochastic gradient descent on $L(\theta)$ in (17)
- 6: **until** converged

Inference Stage:

- 7: for a test input a
 - 8: **for** $n = 1, \dots, N_s$ **do**
 - 9: $u_T^{(n)} \sim \mathcal{N}(0, I)$
 - 10: **for** $t = T, \dots, 1$ **do**
 - 11: $u_{t-1}^{(n)} \sim q_\theta(u_{t-1}|u_t, a)$ in (13)
 - 12: **return** statistics of $\{u_0^{(n)}\}_{n=1}^{N_s}$
-

As a probabilistic model, PDNO learns a class of conditional distributions $q_\theta(\cdot|a)$ rather than the deterministic solution operator. For a given test input a , N_s approximated samples of $u|a$, denoted by $\{\mathcal{S}_\theta^{(n)}(a)\}_{n=1}^{N_s}$, are required in order to obtain various statistics of the conditional distribution. This is the case when we handle noisy data sets. However, it should be emphasized that, in the case of noise-free data where we learn a class of point distribution $\delta_u(\cdot|a)$ concentrated at u , only a single sample is required to estimate the corresponding solution u provided that the model is well trained. In practice, we validate the learned model $\delta_u(\cdot|a)$ with a diagnostic run on the test data set to check whether the estimated standard deviation is approximately zero.

4 Computational benchmarks

We demonstrate efficacy of PDNO on several benchmarks and provide comparison with results obtained by FNO [13]. Denote $\tilde{\mathcal{D}}$ as the test data set. We evaluate the prediction accuracy and uncertainty of the model \mathcal{S}_θ by the mean relative L_2 -error (MRLE) and the mean standard deviation (MSTD) that are defined by

$$\frac{1}{|\tilde{\mathcal{D}}|} \sum_{(a,u) \in \tilde{\mathcal{D}}} \frac{\|\text{mean}(\{\mathcal{S}_\theta^{(n)}(a)\}_{n=1}^{N_s}) - u\|_2}{\|u\|_2} \quad \text{and} \quad \frac{1}{|\tilde{\mathcal{D}}|} \sum_{(a,u) \in \tilde{\mathcal{D}}} \frac{\|\text{std}(\{\mathcal{S}_\theta^{(n)}(a)\}_{n=1}^{N_s})\|_2}{N_s},$$

respectively. All experiments are implemented with a single Tesla T4 GPU. More implementation details about the experiments are given in Appendix C.

Test 1 (Elliptic equation in 1D) We start with a problem whose analytical solution is known explicitly:

$$-(a(x)u'(x))' = 0, \quad x \in (-1, 1), \quad (18)$$

with the boundary condition $u(-1) = 0$ and $u(+1) = 1$, and u' denotes du/dx . We are interested in learning the solution operator \mathcal{S} mapping a log-normal field $a \in \mathcal{A} = L^2((-1, 1); \mathbb{R})$ to the solution

field $u \in \mathcal{U} = L^2((-1, 1); \mathbb{R})$. Details on the data generation and the analytical solution can be found in Appendix C.1.

We apply PDNO in both settings of noise-free data and noisy data. In order to assess the distribution of the learned solution field, we choose two distinct grid points x_1 and x_2 over $(-1, 1)$ and apply the learned PDNO to predict the joint distribution $(u(x_1), u(x_2))$. To generate an approximation to the joint distribution, we first sample $\mathcal{S}_\theta(a)$ for $\tilde{N} = 10^5$ inputs a from the test data set and then evaluate the learned outputs $\mathcal{S}_\theta(a)$ at x_1 and x_2 to obtain $(u_\theta(x_1), u_\theta(x_2))$. In Figure 2, we examine the 2D joint histogram sampled from the exact solution $(u(x_1), u(x_2))$ and the approximated solution $(u_\theta(x_1), u_\theta(x_2))$ based on $\tilde{N} = 10^5$ inputs $a \sim \mu$. The result shows the errors are concentrated at the order of 10^{-5} (see Figure 2 Right). We also test the performance of PDNO on a Gaussian noise data set. Figure A1 in Appendix C.1 demonstrates that PDNO is able to learn the mean as well as the standard deviation from a noisy data set, which is the key advantage of PDNO over other deterministic methods.

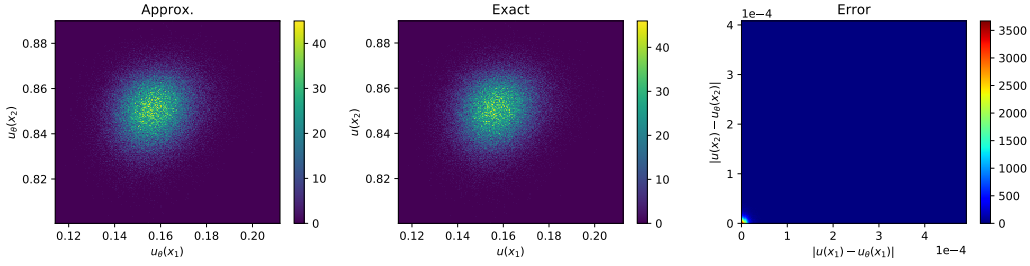


Figure 2: 2D joint histograms of the solution field evaluated at x_1 and x_2 based on $\tilde{N} = 10^5$ test points. **Left:** the histogram of the approximate solution; **Center:** the histogram of the exact solution; **Right:** the histogram of the error, showing the errors at all test points to be roughly of the order 10^{-5} (errors are concentrated at the lower left corner).

Test 2 (Elliptic equation in 2D) To test the method on higher dimensional input-output data sets, we apply the proposed PDNO to learn a solution operator $\mathcal{S} : a \in L^\infty(D; \mathbb{R}) \mapsto u \in H_0^1(D; \mathbb{R})$ to a 2D elliptic PDE:

$$\begin{aligned} -\nabla \cdot (a(x) \nabla u(x)) &= f(x) & x \in D \\ u(x) &= 0 & x \in \partial D, \end{aligned} \quad (19)$$

where the input a is a random field defined in Appendix C.2. See Appendix C.2 for more on simulation parameters and setup of the experiment.

As shown in Table 1, in the noise-free data setting, PDNO achieves lower MRLE than FNO in various mesh sizes. With this example we also present a study for learning the solution operator along with the uncertainty from a noisy data set \mathcal{D}_η in which the output data are corrupted by a Gaussian noise $\eta \sim N(0, \sigma^2 \mathbf{I})$. We present the results in Figure A2 of Appendix C.2 where both the mean and the standard deviation are predicted for a particular input a . Again the result shows that PDNO allows us to learn the solution operator and recover the magnitude of the noise.

Table 1: MRLE and MSTD for the 2D elliptic PDE in Test 2.

Method	Parameter	$M = 64$		$M = 128$		$M = 256$	
		MRLE	MSTD	MRLE	MSTD	MRLE	MSTD
FNO	2, 376, 449	0.0060	N/A	0.0078	N/A	0.0050	N/A
PDNO	35, 707, 841	0.0046	5.08e−07	0.0022	3.52e−07	0.0037	1.21e−05

Test 3 (Burgers’ equation) We consider Burgers’ equation with periodic boundary conditions on the spatial domain $D = (0, 1)$,

$$\begin{aligned}\partial_t u(x, t) + u(x, t)\partial_x u(x, t) &= \nu \partial_{xx} u(x, t), & x \in D, \quad t \in (0, 1] \\ u(x, 0) &= u_0(x), & x \in D\end{aligned}\tag{20}$$

where ν is the viscosity coefficient and $u_0 \in L^2_{\text{per}}(D; \mathbb{R})$ is the random input initial condition whose generation is described in Appendix C.3. Similar to [13], we aim to learn the operator $\mathcal{S} : L^2_{\text{per}}(D; \mathbb{R}) \rightarrow L^p_{\text{per}}(D; \mathbb{R})$, for $p > 1$, mapping the initial condition u_0 to the solution $u(\cdot, 1)$.

Prediction result is summarized in Table 2 and the decay of MRLE is shown in Figure 3. We observed that FNO achieves the claimed mesh invariant property in this example. Although PDNO achieves low MRLE for the experiment, FNO performs significantly better than PDNO in various mesh size. We argue that the great performance of FNO for this example is due to the periodic boundary conditions used in the equation.

Table 2: MRLE and MSTD on Burgers’ equation in Test 3.

Method	Parameter	M=512		M=1024		M=2048	
		MRLE	MSTD	MRLE	MSTD	MRLE	MSTD
FNO	582, 849	0.0005	N/A	0.0005	N/A	0.0005	N/A
PDNO	3, 980, 129	0.0047	5.47e−04	0.0053	7.93e−04	0.0152	1.51e−03

Test 4 (Advection equation) This example aims at investigating the performance of PDNO for an advection PDE whose solution is highly non-smooth. We test our method for the 1D advection equation with the inflow condition on the domain $D = (0, 1)$:

$$\begin{aligned}\partial_t u(x, t) + \partial_x u(x, t) &= 0 & x \in D, \\ u(x, 0) &= u_0(x), \quad \text{and} \quad u(0, t) = 0 & t \geq 0.\end{aligned}\tag{21}$$

The solution operator learned in this problem is the mapping from the initial condition u_0 to a solution at a fixed time $t_f > 0$, i.e., $\mathcal{S} : u_0 \in L^\infty(D; \mathbb{R}) \mapsto u(\cdot, t_f) \in L^\infty(D; \mathbb{R})$. The distribution of the input u_0 is chosen in a way such that the output solution $u(\cdot, t_f)$ is highly non-smooth. See C.4 for more details on the setup.

The results of the experiment are shown in the Table 3 which compares the MRLE obtained by PDNO and FNO. In this challenging example, PDNO significantly outperforms FNO in all mesh sizes. Figure A3 depicts the solutions u learned by FNO and PDNO at particular inputs a . Compared to FNO, our PDNO is able to learn very fine details of the highly non-smooth solution.

Table 3: MRLE and MSTD for the Advection problem in Test 4.

Method	Parameter	M=256		M=512		M=1024	
		MRLE	MSTD	MRLE	MSTD	MRLE	MSTD
FNO	2, 328, 961	0.0514	N/A	0.1072	N/A	0.1325	N/A
PDNO	3, 980, 129	0.0062	7.91e−04	0.0081	7.38e−04	0.0445	2.59e−03

Conclusion

We have presented a probabilistic generative model based on DDPM for learning the solution operator for parametric PDEs. Our method differs from other state-of-the-art approaches in that we view the input-to-output mapping as a family of conditional distributions conditioned on the input parameter. Therefore, our model predicts the solution with quantified uncertainty. While the method has various advantages, we also observed several limitations in numerical experiments.

More specifically, the current method learns a model that is trained on a predefined mesh, which limits the model’s ability to predict solutions at points outside the mesh. More importantly, the

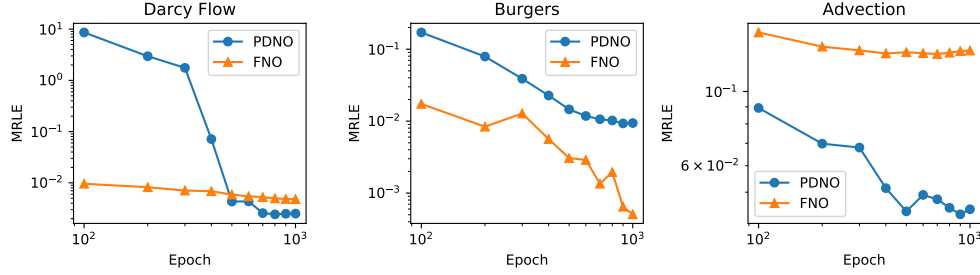


Figure 3: Decay of the MRLE with respect to the number of training epochs. **Left:** Test 2, the 2D elliptic PDE with $M = 128$. **Center:** Test 3, Burgers’ equation with $M = 1024$. **Right:** Test 4, the advection PDE with $M = 1024$.

mesh-dependent property requires us to retrain the model in order to learn over different meshes. Finally, since sampling of $u|a$ requires sequential sampling for T steps, the inference of our model is relatively slow compared to other deterministic models.

To deal with the mesh-dependent issue, we propose to carry out the diffusion learning over an appropriate latent space [20], e.g., over the Fourier space [13] or the spectral space [19]. Alternatively, we can take advantage of the cascaded diffusion model pipeline to make predictions on a fine mesh based on a model pre-trained on a coarse mesh [9]. As for the sampling efficiency, the denoising diffusion implicit models can be applied to accelerate the inference with a slight compromise in accuracy [23]. Finally, the current implementation utilizes a UNet architecture to represent the transition density, which often involves larger number of parameters than the architecture for FNO. A more efficient DDPM based solver calls for a special purpose architecture for the operator learning application.

Acknowledgments and Disclosure of Funding

Research of P.P. was supported by the U.S. Army Research Office Grant W911NF2220234. Computations in this research were supported in part through the use of DARWIN computing system: DARWIN – A Resource for Computational and Data-intensive Research at the University of Delaware and in the Delaware Region, which is supported by NSF under Grant Number: 1919839.

References

- [1] P. Batlle, M. Darcy, B. Hosseini, and H. Owhadi. Kernel methods are competitive for operator learning. *arXiv preprint arXiv:2304.13202*, 2023.
- [2] K. Bhattacharya, B. Hosseini, N. B. Kovachki, and A. M. Stuart. Model reduction and neural networks for parametric pdes. *The SMAI journal of computational mathematics*, 7:121–157, 2021.
- [3] T. Chen and H. Chen. Universal approximation to nonlinear operators by neural networks with arbitrary activation functions and its application to dynamical systems. *IEEE Transactions on Neural Networks*, 6(4):911–917, 1995.
- [4] M. De Hoop, D. Z. Huang, E. Qian, and A. M. Stuart. The cost-accuracy trade-off in operator learning with neural networks. *arXiv preprint arXiv:2203.13181*, 2022.
- [5] P. Dhariwal and A. Nichol. Diffusion models beat gans on image synthesis. *Advances in Neural Information Processing Systems*, 34:8780–8794, 2021.
- [6] G. Gupta, X. Xiao, and P. Bogdan. Multiwavelet-based operator learning for differential equations. *Advances in neural information processing systems*, 34:24048–24062, 2021.
- [7] J. S. Hesthaven and S. Ubbiali. Non-intrusive reduced order modeling of nonlinear problems using neural networks. *Journal of Computational Physics*, 363:55–78, 2018.
- [8] J. Ho, A. Jain, and P. Abbeel. Denoising diffusion probabilistic models. *Advances in Neural Information Processing Systems*, 33:6840–6851, 2020.
- [9] J. Ho, C. Saharia, W. Chan, D. J. Fleet, M. Norouzi, and T. Salimans. Cascaded diffusion models for high fidelity image generation. *J. Mach. Learn. Res.*, 23(47):1–33, 2022.

- [10] V. Khrulkov, G. Ryzhakov, A. Chertkov, and I. Oseledets. Understanding ddpn latent codes through optimal transport. *arXiv preprint arXiv:2202.07477*, 2022.
- [11] N. Kovachki, S. Lanthaler, and S. Mishra. On universal approximation and error bounds for Fourier neural operators. *The Journal of Machine Learning Research*, 22(1):13237–13312, 2021.
- [12] N. Kovachki, Z. Li, B. Liu, K. Azizzadenesheli, K. Bhattacharya, A. Stuart, and A. Anandkumar. Neural operator: Learning maps between function spaces. *arXiv preprint arXiv:2108.08481*, 2021.
- [13] Z. Li, N. Kovachki, K. Azizzadenesheli, B. Liu, K. Bhattacharya, A. Stuart, and A. Anandkumar. Fourier neural operator for parametric partial differential equations. *arXiv preprint arXiv:2010.08895*, 2020.
- [14] Z. Li, N. Kovachki, K. Azizzadenesheli, B. Liu, K. Bhattacharya, A. Stuart, and A. Anandkumar. Neural operator: Graph kernel network for partial differential equations. *arXiv preprint arXiv:2003.03485*, 2020.
- [15] Z. Li, H. Zheng, N. Kovachki, D. Jin, H. Chen, B. Liu, K. Azizzadenesheli, and A. Anandkumar. Physics-informed neural operator for learning partial differential equations. *arXiv preprint arXiv:2111.03794*, 2021.
- [16] L. Lu, P. Jin, and G. E. Karniadakis. Deeponet: Learning nonlinear operators for identifying differential equations based on the universal approximation theorem of operators. *arXiv preprint arXiv:1910.03193*, 2019.
- [17] L. Lu, X. Meng, S. Cai, Z. Mao, S. Goswami, Z. Zhang, and G. E. Karniadakis. A comprehensive and fair comparison of two neural operators (with practical extensions) based on fair data. *Computer Methods in Applied Mechanics and Engineering*, 393:114778, 2022.
- [18] R. G. Patel, N. A. Trask, M. A. Wood, and E. C. Cyr. A physics-informed operator regression framework for extracting data-driven continuum models. *Computer Methods in Applied Mechanics and Engineering*, 373:113500, 2021.
- [19] A. Phillips, T. Seror, M. Hutchinson, V. De Bortoli, A. Doucet, and E. Mathieu. Spectral diffusion processes. *arXiv preprint arXiv:2209.14125*, 2022.
- [20] R. Rombach, A. Blattmann, D. Lorenz, P. Esser, and B. Ommer. High-resolution image synthesis with latent diffusion models. In *Proceedings of the IEEE/CVF Conference on Computer Vision and Pattern Recognition*, pages 10684–10695, 2022.
- [21] O. Ronneberger, P. Fischer, and T. Brox. U-net: Convolutional networks for biomedical image segmentation. In *Medical Image Computing and Computer-Assisted Intervention—MICCAI 2015: 18th International Conference, Munich, Germany, October 5-9, 2015, Proceedings, Part III* 18, pages 234–241. Springer, 2015.
- [22] J. Sohl-Dickstein, E. Weiss, N. Maheswaranathan, and S. Ganguli. Deep unsupervised learning using nonequilibrium thermodynamics. In *International Conference on Machine Learning*, pages 2256–2265. PMLR, 2015.
- [23] J. Song, C. Meng, and S. Ermon. Denoising diffusion implicit models. *arXiv preprint arXiv:2010.02502*, 2020.
- [24] Y. Song and S. Ermon. Generative modeling by estimating gradients of the data distribution. *Advances in Neural Information Processing Systems*, 32, 2019.
- [25] Y. Song, J. Sohl-Dickstein, D. P. Kingma, A. Kumar, S. Ermon, and B. Poole. Score-based generative modeling through stochastic differential equations. *arXiv preprint arXiv:2011.13456*, 2020.
- [26] L. Sun, H. Gao, S. Pan, and J.-X. Wang. Surrogate modeling for fluid flows based on physics-constrained deep learning without simulation data. *Computer Methods in Applied Mechanics and Engineering*, 361:112732, 2020.
- [27] R. Wang, K. Kashinath, M. Mustafa, A. Albert, and R. Yu. Towards physics-informed deep learning for turbulent flow prediction. In *Proceedings of the 26th ACM SIGKDD International Conference on Knowledge Discovery & Data Mining*, pages 1457–1466, 2020.
- [28] S. Wang, Y. Teng, and P. Perdikaris. Understanding and mitigating gradient flow pathologies in physics-informed neural networks. *SIAM Journal on Scientific Computing*, 43(5):A3055–A3081, 2021.
- [29] S. Wang, H. Wang, and P. Perdikaris. Learning the solution operator of parametric partial differential equations with physics-informed deepnets. *Science advances*, 7(40):eabi8605, 2021.
- [30] S. Wang, X. Yu, and P. Perdikaris. When and why pinns fail to train: A neural tangent kernel perspective. *Journal of Computational Physics*, 449:110768, 2022.
- [31] T. Wang and J. Knap. Stochastic deep-ritz for parametric uncertainty quantification. *arXiv preprint arXiv:2206.00867*, 2022.
- [32] C. K. Williams and C. E. Rasmussen. *Gaussian processes for machine learning*, volume 2. MIT press Cambridge, MA, 2006.

- [33] Y. Zhu and N. Zabaras. Bayesian deep convolutional encoder–decoder networks for surrogate modeling and uncertainty quantification. *Journal of Computational Physics*, 366:415–447, 2018.
- [34] Y. Zhu, N. Zabaras, P.-S. Koutsourelakis, and P. Perdikaris. Physics-constrained deep learning for high-dimensional surrogate modeling and uncertainty quantification without labeled data. *Journal of Computational Physics*, 394:56–81, 2019.

A Key notations

For quick reference, important notations are summarized in the following table.

Table A1: Table of notations

Notation	Definition
T	Number of diffusion timesteps
\mathcal{F}	The mapping that defines the abstract PDE in (1)
\mathcal{A}	Function spaces of input functions a
\mathcal{U}	Function spaces of output functions u
M	Number of grid points per discretization dimension
\mathcal{A}_M	\mathbb{R}^{M^d} , i.e., the discretization mesh for a
\mathcal{U}_M	\mathbb{R}^{M^d} , i.e., the discretization mesh for u
D	The physical space of the abstract PDE in (1)
D_M	Discretized domain of D with an M^d point grid
a	Input that takes value in \mathcal{A} or \mathcal{A}_M
u	Output that takes values in \mathcal{U} or \mathcal{U}_M , same as the initial state u_0
μ	The probability measure induced by a
\mathcal{S}_θ	The parametric approximate operator
\mathcal{S}	The true operator
$q_\theta(\cdot a)$	The parametric conditional model
$p(\cdot a)$	The true conditional model
$q_\theta(u_{t-1} u_t, a)$	The parametric transition density for the reverse time Markov chain
$p(u_{t-1} u_t, a)$	The true transition density for the reverse time Markov chain
$\delta_u(\cdot a)$	The conditional Dirac measure centered at u
ϵ_t	Standard Gaussian noise (at time t)
\mathcal{D}	Noise free training data set of input-output pairs
\mathcal{D}_η	Noisy training data set whose outputs are corrupted by $\eta \sim \mathcal{N}(0, \sigma^2 \mathbf{I})$
$\tilde{\mathcal{D}}$	Noise free testing data set
N	Number of training samples, i.e., $ \mathcal{D} $ or $ \mathcal{D}_\eta $
\tilde{N}	Number of testing samples, i.e., $ \tilde{\mathcal{D}} $

B Mathematical derivations of PDNO

B.1 Decomposition of the conditional VLB

We outline the derivation of the conditional VLB (11) which is at the basis of constructing the network approximation of the reverse process. The derivation follows similar principles as for the unconditional DDPM, nonetheless, we present it here for the sake of completeness. We recall that we are constructing a parametrized approximation of the original distribution $p(u_0|a)$ using the distribution $q_\theta(u_0|a)$ of the reverse process, conditioned on the input data a . First, note that

$$\begin{aligned}\log q_\theta(u_0|a) &= \mathbb{E}_{p(u_0|a)}[\log q_\theta(u_0|a)] \\ &= \mathbb{E}_{p(u_0|a)}\left[\log \int_{u_T} \dots \int_{u_1} q_\theta(u_{0:T}|a) du_{1:T}\right] \\ &= \mathbb{E}_{p(u_0|a)}\left[\log \mathbb{E}_{p(u_{1:T}|u_0)}\left[\frac{q_\theta(u_{0:T}|a)}{p(u_{1:T}|u_0)}\right]\right].\end{aligned}$$

Applying Jensen's inequality to the inner expectation leads to the following conditional VLB

$$-\log q_\theta(u_0|a) \leq -\text{VLB} = \mathbb{E}_{p(u_{0:T}|a)}\left[\log \frac{p(u_{1:T}|u_0)}{q_\theta(u_{0:T}|a)}\right].$$

The decomposition (11) then follows directly from the Markov property and the Bayes' formula

$$\begin{aligned}-\text{VLB} &= \mathbb{E}_{p(u_{0:T}|a)}\left[-\log q_\theta(u_T) + \sum_{t=2}^T \log \frac{p(u_t|u_{t-1})}{q_\theta(u_{t-1}|u_t, a)} + \log \frac{p(u_1|u_0)}{q_\theta(u_0|u_1, a)}\right] \\ &= \mathbb{E}_{p(u_{0:T}|a)}\left[\log \frac{p(u_T|u_0)}{q_\theta(u_T)}\right] + \sum_{t=2}^T \mathbb{E}_{p(u_{0:T}|a)}\left[\log \frac{p(u_{t-1}|u_t, u_0)}{q_\theta(u_{t-1}|u_t, a)}\right] + \mathbb{E}_{p(u_{0:T}|a)}[-\log q_\theta(u_0|u_1, a)] \\ &= L_T + \sum_{t=2}^T L_{t-1} + L_0,\end{aligned}$$

where we used the fact that for $t = 2, \dots, T-1$,

$$\mathbb{E}_{p(u_{0:T}|a)}\left[\log \frac{p(u_{t-1}|u_t, u_0)}{q_\theta(u_{t-1}|u_t, a)}\right] = \mathbb{E}_{p(u_t, u_0|a)}\mathbb{E}_{p(u_{t-1}|u_t, u_0)}\left[\log \frac{p(u_{t-1}|u_t, u_0)}{q_\theta(u_{t-1}|u_t, a)}\right] = L_{t-1}$$

and

$$\mathbb{E}_{p(u_{0:T}|a)}\left[\log \frac{p(u_T|u_0)}{q_\theta(u_T)}\right] = \mathbb{E}_{p(u_0|a)}\mathbb{E}_{p(u_T|u_0)}\left[\log \frac{p(u_T|u_0)}{q_\theta(u_T)}\right] = L_T.$$

B.2 Derivation of the reverse transition distribution

We derive the true reverse transition density (12) and the associated epsilon parameterization. Since

$$p(u_t|u_0) = \int p(u_t|u_{t-1}) \dots p(u_1|u_0) du_1 \dots du_{t-1},$$

the convolution of t Gaussian densities gives

$$p(u_t|u_0) = \mathcal{N}(u_t; \sqrt{\bar{\alpha}_t}u_0, (1 - \bar{\alpha}_t)\mathbf{I}), \quad (\text{B.1})$$

where $\bar{\alpha}_t = \prod_{n=1}^t \alpha_n$ with $\alpha_t = 1 - \beta_t$. To derive the reverse transition probability (12), we apply Bayes' formula to obtain

$$p(u_{t-1}|u_t, u_0) = p(u_t|u_{t-1}) \frac{p(u_{t-1}|u_0)}{p(u_t|u_0)} = \mathcal{N}(u_{t-1}; m(t, u_t, u_0), \Sigma(t, u_t, u_0)),$$

with

$$m(t, u_t, u_0) = \frac{\sqrt{\bar{\alpha}_t}(1 - \bar{\alpha}_{t-1})}{1 - \bar{\alpha}_t}u_t + \frac{\sqrt{\bar{\alpha}_{t-1}}\beta_t}{1 - \bar{\alpha}_t}u_0, \quad \Sigma(t, u_t, u_0) = \frac{1 - \bar{\alpha}_{t-1}}{1 - \bar{\alpha}_t}\beta_t\mathbf{I}.$$

Now we can take advantage of the re-parameterization of u_0 , i.e.,

$$u_0 = \frac{1}{\sqrt{\bar{\alpha}_t}}(u_t - \sqrt{1 - \bar{\alpha}_t}\epsilon_t), \quad (\text{B.2})$$

to re-parameterize the mean in terms of the Gaussian noise ϵ_t as

$$m(t, u_t, u_0) = \frac{1}{\sqrt{\bar{\alpha}_t}}\left(u_t - \frac{1 - \alpha_t}{\sqrt{1 - \bar{\alpha}_t}}\epsilon_t\right), \quad \Sigma(t, u_t, u_0) = \frac{1 - \bar{\alpha}_{t-1}}{1 - \bar{\alpha}_t}\beta_t\mathbf{I}.$$

Therefore, DDPM indeed learns a noise predictor ϵ_θ that approximates the Gaussian noise ϵ_t with neural networks at each timestep. This *epsilon* parameterization has been experimentally observed to outperform the direct parameterization of the mean $m(t, u_t, u_0)$.

B.3 The choice of the covariance for the reverse process

We justify the covariance parameterization (14) using basic techniques of information theory. Let X and Y be two random variables supported by \mathcal{X} and \mathcal{Y} , respectively. We denote $H_p(X) = -\int_{\mathcal{X}} p_X(x) \log p_X(x) dx$ the entropy of $X \sim p_X(x)$. We recall the conditional entropy of Y given X is defined as

$$H_p(Y|X) = -\int_{x \in \mathcal{X}} \int_{y \in \mathcal{Y}} p_{(X,Y)}(x,y) \log p_{Y|X=x}(y|x) dx dy,$$

where $p_{(X,Y)}$ is the joint density of (X, Y) and $p_{Y|X=x}$ is the density of Y conditioned on $X = x$. Furthermore, we recall the definition of mutual information between X and Y

$$I(X; Y) = I(Y; X) = H_p(X) + H_p(Y) - H_p(X, Y)$$

where $H(X, Y)$ is the entropy of the joint distribution $p_{(X,Y)}(x, y)$.

Noise-free data. The following proposition gives the conditional entropy of the reverse transition $H_p(u_{t-1}|u_t)$ in the case of noise-free data.

Proposition 1. *Let $u_{0:T}$ be a Markov chain with a transition probability defined by (5). Suppose that the initial state u_0 follows a Dirac distribution at a point u_0 , i.e., $u_0 \sim \delta_{u_0}$, then*

$$H_p(u_{t-1}|u_t) = H_p(u_t|u_{t-1}) + H_p(u_{t-1}|u_0) - H_p(u_t|u_0), \quad t = 1, \dots, T.$$

Proof. For $t = 1, \dots, T$, applying the data processing inequality to the Markov chain $u_0 \rightarrow u_{t-1} \rightarrow u_t$ we have

$$I(u_0; u_{t-1}) \geq I(u_0; u_t). \quad (\text{B.3})$$

Furthermore, from the definition of the mutual information, we have

$$I(u_0; u_{t-1}) = H_p(u_{t-1}) - H_p(u_{t-1}|u_0),$$

$$I(u_0; u_t) = H_p(u_t) - H_p(u_t|u_0)$$

where $H_p(u_t) = -\int p_{u_t}(u) \log p_{u_t}(u) du$ is the entropy of u_0 . Hence, we obtain in terms of conditional entropies

$$H_p(u_t) - H_p(u_{t-1}) \leq H_p(u_t|u_0) - H_p(u_{t-1}|u_0).$$

Owing to the fact that (from the symmetry $I(u_{t-1}|u_t) = I(u_t|u_{t-1})$)

$$H_p(u_t) - H_p(u_{t-1}) = H_p(u_t|u_{t-1}) - H_p(u_{t-1}|u_t),$$

we immediately obtain the inequality

$$H_p(u_{t-1}|u_t) \geq H_p(u_t|u_{t-1}) + H_p(u_{t-1}|u_0) - H_p(u_t|u_0)$$

Note that the inequality (B.3) is attained if and only if $u_0 \rightarrow u_t \rightarrow u_{t-1}$ also forms a Markov chain, i.e.,

$$p(u_{t-1}|u_t, u_0) = p(u_{t-1}|u_t), \quad (\text{B.4})$$

which holds true when $u_0 \sim \delta_{u_0}$, where δ_{u_0} is the Dirac measure supported at u_0 . □

An important implication of the above proposition is the parameterization of the reverse process covariance (14). When $u_0 \sim \delta_{u_0}$, the Markov property (B.4) holds and hence (12) is independent of u_0 . In this case, the parameterization (14) for $\Sigma_\theta(t, u_t, a)$ in the noise free setting is optimal in the sense that $H_p(u_{t-1}|u_t) = H_{q_\theta}(u_{t-1}|u_t)$.

Gaussian noise data. A similar result holds in the case of data perturbed by an additive Gaussian noise.

Proposition 2. *Let $u_{0:T}$ be a Markov chain with transition probability defined by (5). Suppose that the initial state u_0 follows a (nonzero mean) Gaussian distribution with the identity covariance, i.e., $u_0 \sim \mathcal{N}(m, \mathbf{I})$, then*

$$H_p(u_{t-1}|u_t) = H_p(u_t|u_{t-1}), \quad t = 1, \dots, T.$$

Proof. The identity follows from the well-know property that the Gaussian distribution $\mathcal{N}(m, \mathbf{I})$ has the maximum entropy among all distributions whose density is strictly positive on \mathbb{R}^n and is subject to the identity covariance constraint. The forward transition (5) preserves the identity covariance of the forward DDPM since

$$\text{Cov}(u_t) = \beta_t \text{Cov}(u_{t-1}) + (1 - \beta_t) \text{Cov}(\epsilon_t) = \mathbf{I}.$$

Therefore, $H_p(u_t) = H_p(u_{t-1})$ for all $t = 1, \dots, T$, which immediately implies the desired equality since

$$H_p(u_{t-1}) - H_p(u_{t-1}|u_t) = H_p(u_t) - H_p(u_t|u_{t-1}).$$

□

The result suggests that the DDPM learns a transformation between $\mathcal{N}(m, \mathbf{I})$ and $\mathcal{N}(0, \mathbf{I})$, which indeed corresponds to the optimal transport map between the two Gaussians [10]. Furthermore, after integrating out u_0 in (12), the true reverse distribution $p(u_{t-1}|u_t)$ has a covariance $\beta_t \mathbf{I}$. Hence, the parameterization (14) for Σ_θ in the Gaussian noise setting is optimal in the sense that $H_p(u_{t-1}|u_t) = H_{q_\theta}(u_{t-1}|u_t)$.

In both cases, the noise-free and Gaussian noise, the learned parametric model q_θ achieves the exact likelihood under the true model p , i.e.,

$$\mathbb{E}_{q_\theta} [-\log q_\theta(u_{0:T})] = H_{q_\theta}(u_T) + \sum_{t=1}^T H_{q_\theta}(u_{t-1}|u_t) = H_p(u_T) + \sum_{t=1}^T H_p(u_{t-1}|u_t) = \mathbb{E}_p [-\log p(u_{0:T})].$$

C More details on computational benchmarks

We provide further details about data generation, training, and testing of PDNO for the test problems. Before we present the detailed setup of each test problem, we remind the reader about the following general setup for all test problems presented:

- The data set is obtained by sampling inputs, i.e., the fields $a \in \mathcal{A}$ and then solving the corresponding equation $\mathcal{F}(u; a) = 0$ in order to obtain the output $u \in \mathcal{U}$.
- The sampling distribution $a \sim \mu$ generally depends on a specific model. In the tests reported here as well as in [13], the input fields a are sampled from random fields that are obtained by transformations of Gaussian fields of mean zero, with a given covariance operator described for each test separately.
- Recall that we use the same notation for the finite dimensional approximation to a and u on finite meshes representing the fields by their grid values, i.e., $a = a|_{D_M} \in \mathbb{R}^{M^d}$ and $u = u|_{D_M} \in \mathbb{R}^{M^d}$, thus the dimensions of the input and output spaces are determined by the number of grid points per dimension M and the dimension of the domain d .
- The training data set $\mathcal{D} = \{(a^{(i)}, u^{(i)})\}_{i=1}^N$ is built from N samples of a . Similarly a testing data set $\tilde{\mathcal{D}}$ is generated with \tilde{N} testing pairs.
- The sequential sampling of the reverse Markov chain is represented by a UNet backbone whose parameters are shared across all time steps $t = 1, \dots, T$. The sinusoidal position encoding is used to specify the diffusion time t .
- We use a multi-head self-attention block that connects the up-scaling and down-scaling blocks of the UNet. However, we found the impact of the self-attention block is inconsequential to the final computational accuracy.
- Comparing to the unconditional DDPM, the proposed PDNO takes an additional argument a for the noise predictor $\epsilon_\theta(t, u_t, a)$. Since a and u_t are of the same dimension in general, we simply apply channel wise concatenation for a and u_t before we feed them into the UNet. However, we emphasize that the architecture can be readily modified to handle a and u_t that are of different spatial dimensions through projecting them into a common latent space.

C.1 Test 1: Elliptic equation in 1D

The random input field in this example corresponds to the log-normal field $a(x) = e^{\beta V(x)}$ with $\beta = 0.1$, where the potential V is parameterized by a random vector $(A_1, \dots, A_n, B_1, \dots, B_n)$, namely,

$$V(x) = \frac{1}{\sqrt{n}} \sum_{k=1}^n A_k \cos(\pi k x) + B_k \sin(\pi k x),$$

where A_k and B_k are independent standard normal random variables. In this example, we choose $n = 5$ and thus the log-normal random field is parameterized by 10 independent Gaussians. One can easily verify that $V(x)$ is a Gaussian random field with zero mean and the covariance kernel

$$\text{cov}(x_1, x_2) = n^{-1} \sum_{k=1}^n \cos(\pi k(x_2 - x_1)).$$

By direct calculation it can be easily verified that the exact solution of the problem (18) is

$$u(x) = \left(\int_{-1}^1 a^{-1}(\xi) d\xi \right)^{-1} \int_{-1}^x a^{-1}(\xi) d\xi.$$

To generate the input-output pairs for training and testing, we apply the above formula with numerical integration. We generate $N = 10^4$ pairs for the noise-free training set \mathcal{D} and another $\tilde{N} = 10^4$ pairs for the noise-free

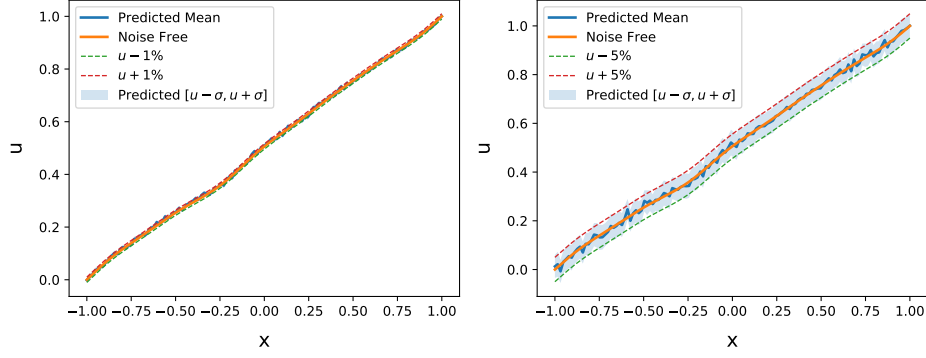


Figure A1: Solutions to the 1D elliptic equation in Test 1 learned by PDNO. The model is trained on a data set corrupted by an additive Gaussian noise $\mathcal{N}(0, \sigma^2 \mathbf{I})$. **Left:** the predicted mean and confidence interval of the solution u corresponds to a particular input a . The model is trained on the noisy data set with $\sigma = 1\%$. **Right:** the predicted mean and confidence interval of the solution u corresponds to a particular input a . The model is trained on the noisy data set with $\sigma = 5\%$. The predicted confidence intervals (blue shaded band) learned by PDNO coincides the theoretical confidence intervals (lower bound and upper bound indicated by green dashed line and red dashed line, respectively).

testing set $\tilde{\mathcal{D}}$, which are used to train PDNO whose accuracy is reported in Figure 2. The noisy data set $\mathcal{D}_\eta = \{(a^{(n)}, u_\eta^{(n)})\}_{n=1}^N$ is generated by corrupting the output u with a Gaussian noise $\eta \sim \mathcal{N}(0, \sigma^2 \mathbf{I})$, i.e.,

$$u_\eta = u + \eta.$$

We also train our PDNO on the noisy data set and validate it on the noise-free test data set $\tilde{\mathcal{D}}$. The predicted mean and standard deviation are reported in Figure A1. Set of hyper-parameters used for training the PDNO is summarized in Table A2.

Table A2: Training hyper-parameters for Test 1. Elliptic equation in 1D

Architecture	
Initial base channels	32
Up/down sampling multiplier	(1, 2, 4, 8)
Residual blocks per resolution	2
Training	
Timesteps T	100
Epochs	1000
Batch size	50
# of training points N	10000
Noise schedule	cosine
Optimizer	Adam
Learning rate	1e−4 initially; halved by half per 100 epochs
Data normalized	No
Testing	
# of testing points \tilde{N}	10000
# of samples N_s	1 if noise-free; 500 if noisy

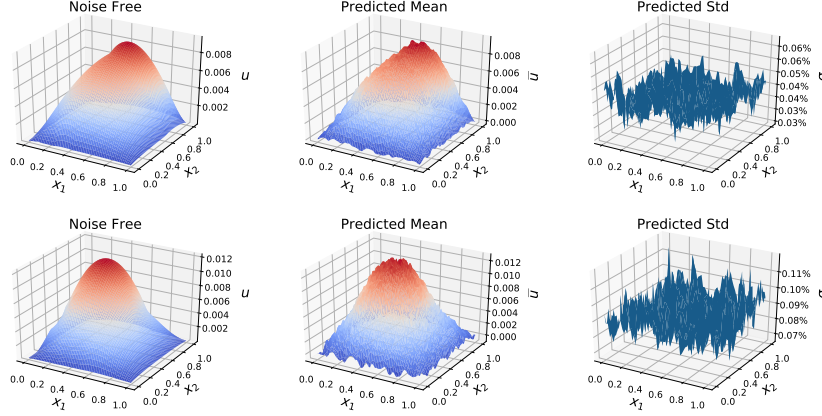


Figure A2: Solutions to the 2D elliptic PDE in Test 2 learned by PDNO. The model is trained on a data set corrupted by an additive zero-mean Gaussian noise $\mathcal{N}(0, \sigma^2 \mathbf{I})$. **Top:** the predicted mean and std of the solution u corresponds to a particular input a . The model is trained on the noisy data set with $\sigma = 0.0005$. **Bottom:** the predicted mean and std of the solution u corresponds to a particular input a . The model is trained on the noisy data set with $\sigma = 0.001$. The noise values correspond to the error of 5% and 10% at the maximum values (≈ 0.01) of the solution u .

C.2 Test 2: Elliptic equation in 2D

In this example, the random input a is obtained from the Gaussian field $\tilde{a}(x)$ by

$$a(x) = \alpha + (\beta - \alpha) \mathbb{1}_{\{\tilde{a}(x) \geq 0\}}.$$

The Gaussian field \tilde{a} has mean zero and covariance operator $(-\Delta + \tau^2)^{-r}$, where Δ is the Laplace operator with Neumann boundary conditions on D . Note that τ defines the inverse correlation length and r controls the regularity of the field.

In correspondence to experiments reported in [13] we have chosen $\tau = 3$, $r = 2$, and $\alpha = 4$, $\beta = 12$. The right hand side was $f(x) \equiv 1$. All functions in this example are represented by their grid values on the mesh of the size $M \times M$, thus the dimension of the data points is M^2 . The size of meshes used in the experiments and the corresponding prediction result are reported in Table 1. Set of parameters used for training the PDNO is summarized in Table A3.

C.3 Test 3: Burgers' equation

In this experiment, the random input a is the initial condition u_0 that is chosen to be a zero mean Gaussian random field with the covariance operator $625(-\Delta + 25I)^{-2}$ with Neumann boundary conditions. The viscosity is set to $\nu = 1$. The same example is considered in [13] and we use the same data set \mathcal{D} provided in [13] in order to make a performance comparison of our PDNO with the FNO. Set of hyper-parameters used for training PDNO is summarized in Table A4.

C.4 Test 4: Advection equation

The random input field a of the data set is identified with the initial condition

$$u_0 = \mathbb{1}_{\{\tilde{a} \geq 0\}},$$

where \tilde{a} is a Gaussian random field of mean zero and with the covariance kernel $(-\partial_{xx} + \tau^2)^{-r}$. Here the Laplace operator ∂_{xx} is with the zero Neumann boundary conditions. For comparison with the FNO method and results in [4], we use the same values $\tau = 100$ and $r = 2$. The output field of the data set is the solution $u(x, t_f)$ at $t_f = 0.5$ and $x \in (0, 1)$. All functions in this example are represented by their grid values on the mesh of the size M . The size of meshes used in the experiments and the corresponding prediction result are reported in Table 3. Solutions at particular inputs a are presented in Figure A3. Set of parameters used for training PDNO is summarized in Table A5.

Table A3: Training hyperparameters for Test 2. Elliptic equation in 2D

Architecture	
Initial base channels	64
Up/down sampling multiplier	(1, 2, 4, 8)
Residual blocks per resolution	2
Training	
Timesteps T	100
Epochs	1000
Batch size	20
# of training points N	1000
Noise schedule	cosine
Optimizer	Adam
Learning rate	1e−4 initially; halved by half per 100 epochs
Data normalized	Yes
Testing	
# of testing points \tilde{N}	100
# of samples N_s	1 if noise-free; 100 if noisy

Table A4: Training hyperparameters for Test 3. Burgers' equation

Architecture	
Initial base channels	32
Up/down sampling multiplier	(1, 2, 4, 8)
Residual blocks per resolution	2
Training	
Timesteps T	100
Epochs	1000
Batch size	32
# of training points N	1024
Noise schedule	linear
Optimizer	Adam
Learning rate	1e−4 initially; halved by half per 100 epochs
Data normalized	No
Testing	
# of testing points \tilde{N}	1024
# of samples N_s	1

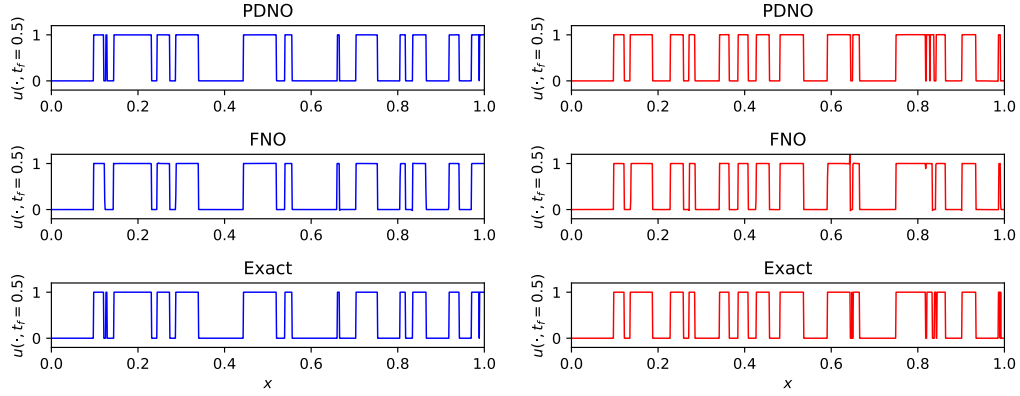


Figure A3: Solutions to the Advection problem at $t_f = 0.5$, i.e., $u(\cdot, 0.5)$ predicted by learned models for particular initial condition inputs u_0 from the test data set. **Left:** solution $u(\cdot, 0.5)$ corresponds to u_0 for which PDNO solution exhibits the lowest MRLE. **Right:** solution $u(\cdot, 0.5)$ corresponds to u_0 for which PDNO solution exhibits the largest MRLE.

Table A5: Training hyperparameters for Test 4. Advection PDE

Architecture	
Initial base channels	32
Up/down sampling multiplier	(1, 2, 4, 8)
Residual blocks per resolution	2
Training	
Timesteps T	100
Epochs	1000
Batch size	20
# of training points N	1500
Noise schedule	cosine
Optimizer	Adam
Learning rate	$8e-5$ fixed
Data normalized	No
Testing	
# of testing points \tilde{N}	300
# of samples N_s	1